JOURNAL OF APPLIED ELECTROCHEMISTRY 23 (1993) 1187–1195

Thin metal oxide films on transparent substrates for Li-insertion devices

S. PASSERINI, J. SCARMINIO*, B. SCROSATI, D. ZANE, F. DECKER

Chemistry Department, University "La Sapienza", Roma, Italy

Received 27 November 1992; revised 12 March 1993

Lithium insertion in metal oxides is a process of interest in many electrochemical applications, including rechargeable batteries and electrochromic displays. In this work we have examined the characteristics of this process in a series of oxides prepared in the thin-film configuration. The lithium insertion process has been examined in WO_3, NiO_x, V_2O_5, Nb_2O_5 and tin-doped indium oxide (ITO) thin film electrodes deposited on transparent substrates. We have considered various aspects of the insertion process in these oxides with particular attention to charge capacity, reversibility, kinetics, structural and optical changes. The results suggest that the process may induce irreversible modifications in some of the host structures. However, under certain well defined conditions, the process occurs reversibly and thus some of the studied oxides may find successful application in electrochemical devices of prime technological interest.

1. Introduction

Lithium insertion compounds are a class of electrodes which have been extensively studied for a variety of electrochemical applications. The main driving force behind this interest has been the application of these compounds as convenient cathodes in rechargeable lithium batteries. Since these batteries are usually designed for high capacity and high energy output, most commonly the insertion electrodes have been prepared and characterized in bulk, pellet-like configurations. Accordingly, the characteristics and properties of the electrochemical lithium insertion processes in bulk metal oxides have been reviewed and discussed in many past [1–4] and recent [5,6] publications.

Less attention has been devoted to the lithium insertion process in thin-film oxide electrodes [7–9], in spite of the fact that the thin film configuration has the advantage of offering a large geometrical and real active area combined with a small amount of active material. Thus, lithium-inserted metal oxide films may find unique applications, such as flexible electrodes for flat batteries for memory back-up in credit cards and portable computers. Furthermore, oxide films with thickness of the order of 0.3 μm or less are often transparent or at least capable of transmitting part of the visible radiation, and this offers the possibility of exploiting the lithium-inserted, thin-film oxide electrodes for various applications related to solar energy conversion, glazing and optical displays. In such a thin film the inserted lithium ions diffuse across a short distance and quasi-equilibrium discharge curves are obtained in less time than with pellets of the bulk oxides. It therefore seemed important to examine in some detail the electrochemical and the optical characteristics of the lithium insertion process in a series of metal oxide electrodes, namely WO_3, NiO_x, V_2O_5 and Nb_2O_5, all prepared in the thin film form (less than 1 μm thickness). Also the plain indium-tin oxide (ITO) film has been added to the family, since there are some indications in the literature that ITO itself is a good host for lithium insertion [10,11]. These oxides are non-lithiated when as-grown, and the electrochemical lithium insertion process will be described. In this paper we seek the relationship between charge capacity and the electrochemical and optical properties, the diffusion kinetics and the transmittance and mechanical stress of the inserted oxide films.

2. Experimental details

The NiO_x, V_2O_5, and NbO_x thin film electrodes were obtained following the procedures described in [9,12] which basically involve reactive d.c. magnetron sputtering in an $Ar–O_2$ atmosphere onto transparent and conductive indium tin oxide (ITO) cover glass sheets. The oxide samples were deposited onto unheated substrates and, as determined by X-ray diffraction analyses, the majority of them are amorphous or nanocrystalline. Only the V_2O_5 samples could be obtained in both the amorphous and crystalline form, by heating the glass substrate to 300 °C. The WO_3 amorphous samples were obtained by evaporation onto the same transparent and conductive ITO-coated glass. Finally, the indium-tin oxide samples were commercial products obtained by IST-Bekaert (Zulte, Belgium). These samples, which consisted of a film typically 0.1 μm thick and with a sheet resistance of 60 Ω/square (corresponding to a resistivity of

* Permanent address: Dep. de Fisica, Univ. Est. de Londrina, Londrina PR, Brasil.

0021-891X

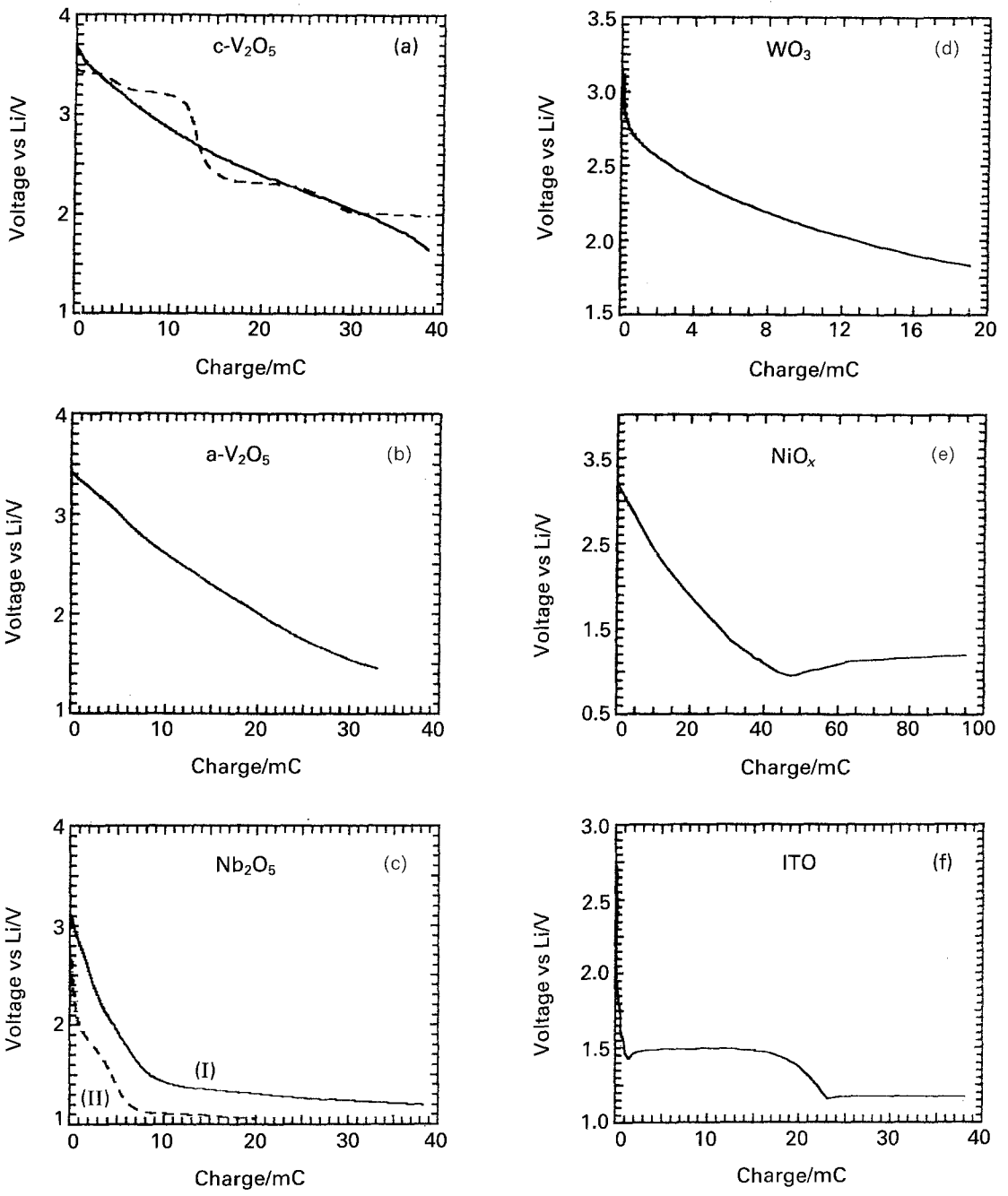

Fig. 1. (a) Potential against charge curve for a crystalline V_2O_5 film (0.15 μm thick, electrode area 0.7 cm^2) during galvanostatic insertion. Insertion current: 5 μA. Dashed line: 1st cycle; solid line: 2nd cycle. (b) Same as above, but for an amorphous V_2O_5 film with area 0.8 cm^2. All other parameters unchanged. (c) Same as above, but for NbO_x film thickness 0.15 μm, area 0.8 cm^2). Insertion current: 5 μA. Solid line: as grown. Dashed line: after heat treatment for 40 h at 380 °C in air. (d) Potential against charge curve for an evaporated WO_3 thin film electrode (thickness 0.3 μm, geometric area 54 cm^2) during galvanostatic lithium insertion at 5 μA. (e) Same as Fig. 1(a), for a NiO_x film (0.06 μm thick, area 4.5 cm^2). Insertion current: 5 μA. (f) Same as in Fig. 1(a), but for a commercial (see text) ITO film (thickness 0.1 μm, area 1 cm^2). Insertion current: 5 μA.

$6 \times 10^{-4}\,\Omega$ cm), sputtered on a 175 mm thick Mylar substrate, were used as received.

The *in situ* electrochemical and optical measurements were performed using a three-electrode cell, having a lithium foil for both the reference and the counter electrode. The cell reservoir consisted of a Teflon hollow cylinder with four optical windows at right angles. The cell was filled with a non-aqueous electrolyte consisting of a 1 M lithium perchlorate solution in propylene carbonate (here abbreviated as $LiClO_4$–PC) and sealed in a controlled atmosphere dry box (humidity content less than 10 p.p.m.) immediately before all the experiments. To drive the electrochemical tests, an Amel 551-galvanostat and an Amel 567 ramp generator were used. The analogue instruments were controlled by means of a Mac II Cl personal computer, which recorded and processed the optical and electrochemical data. The ac impedance measurements were obtained by a Solartron 1250 frequency response analyser coupled with a Solartron 1286 electrochemical interface, both controlled by an HP Vectra computer. The impedance data were fitted using a modified version of the Boukamp fitting program [13]. The measurements of the optical transmittance and of the mechanical stress were obtained by cutting the electrodes,

typically 30 mm long and 3 mm wide and clamping them by the upper end above the electrolyte level. A green argon laser beam ($\lambda = 514.5$ nm) was directed to the lower end of such electrodes, this allowing the simultaneous determination of transmittance and stress by means of an optical set-up described in detail elsewhere [14,15]. All the values of transmittance quoted in this work refer to the system formed by cell + electrolyte + electrode, taking 100% as the transmittance of the system cell + electrolyte.

3. Results and discussion

3.1. *Voltage-charge curves*

The lithium insertion process in the various M_yO_z metal oxide electrodes:

$$xLi^+ + M_yO_z + xe^- \Rightarrow Li_xM_yO_z \qquad (1)$$

was examined in cells of the type:

$$Li|LiClO_4-PC|M_yO_z, \quad ITO\text{–glass} \qquad (2)$$

using a lithium counter electrode, a Li^+ ion conducting liquid electrolyte, i.e. a solution of $LiClO_4$ in propylene carbonate, and a lithium reference electrode. The lithium insertion was promoted in two different ways, namely: (i) by fixed cathodic current (galvanostatic discharge); and (ii) by fixed potential (potentiostatic discharge).

Most of the oxide electrodes showed an open circuit voltage (o.c.v.) value between 3.0 V and 3.5 V against lithium in their pristine state. As expected, the voltage decreased upon lithium ion insertion. However the extent of the voltage decay upon Li insertion varied greatly from oxide to oxide. Figure 1(a) to (f) refer to the voltage-charge curves of the various oxide films during a 'slow' galvanostatic discharge which takes typically several hours. Figure 1(a) shows voltage-composition curves related to the lithium insertion process in the vanadium oxide polycrystalline films, run at a fixed cathodic current of 7 mA cm^{-2}.

The figure clearly shows that in the first cycle (dashed line) the voltage trend develops upon discharge with a series of plateaux separated by regions where the voltage drops abruptly. This can be attributed to the formation of well defined crystalline single phases (at the steps) separated by mixed structures (at the plateaux) where two different phases co-exist. However, in the second cycle (solid line in Fig. 1(a)) the process is represented by a continuous decay indicating that the large lithium uptake completely destroys the initial crystal structure. Subsequent steady-state cycles are those associated with an amorphous electrode. Indeed, if amorphous V_2O_5 samples are used initially, the first lithium insertion cycle develops with a step-free, continuous voltage decrease as the lithium content increases (Fig. 1(b)). This behavior during insertion is very similar to that shown by bulk vanadium pentoxide crystalline [16] and amorphous [17] electrodes. Due to this similarity it is possible to deduce the real composition of the polycrystalline film at the foot of the first large potential step. This is LiV_2O_5 for a charge of 22 mC cm^{-2}, which is in agreement with a simple calculation based on Faraday's law taking the film density to be the same as for the bulk oxide. Care should be taken in analogous assignments of the Li/M_yO_z value for all the amorphous oxide films because it is known that their density may be much less than that of the parent oxide crystals, depending on their preparation.

It is interesting that the lithium insertion in V_2O_5 electrodes proceeds up to charges of the order of 57 mC cm^{-2} (corresponding to 380 mC cm^{-2} μm^{-1}, considering the film thickness), which corresponds to about 2.6 Li atoms per mole of V_2O_5, for a voltage range of 1.5–2 V, namely from 3.5 to 2 V for the crystalline and from 3.5 to 1.5 V for the amorphous sample. Furthermore, we [18] and others [17,19] have observed that amorphous V_2O_5 appears to have a higher reversible lithium capacity than crystalline V_2O_5.

Another voltage-charge trend, typical of an amorphous electrode sample, is that shown by niobium oxide (Fig. 1(c), solid line). However, thermal treatment following film deposition introduces some structure to this oxide, probably due to a partial recrystallization or to a phase change during the annealing procedure. In fact, the voltage-charge curve of the annealed (Fig. 2, dashed line) shows a certain step-like behaviour. However, while the Li-uptake charge for the amorphous sample extends to about 50 mC cm^{-2} (i.e., a value comparable with that of the V_2O_5 electrode) the Li-uptake of the annealed sample is limited to about 25 mC cm^{-2}.

The voltage-charge behaviour of tungsten oxide is again that typical of a single-phase, amorphous electrode (Fig. 1(d)). In this case the galvanostatically-run curve extends to a charge of about 20 mC cm^{-2} in a voltage range of 1 V (2.9–1.9 V). This amorphous material has previously been studied by several authors in the past [20–24]. In particular the voltage-charge curves have been studied with a specific model involving the variation of the electron energy with concentration in the case of sodium guest ions [25].

More complicated is the voltage-charge curve shown by the nickel oxide sample (Fig. 1(e)) where a dip can be observed at rather high lithium concentration (at about 10 mC cm^{-2}). This behaviour, which was observed in previous work [26], may be explained by assuming that high lithium content induces in the oxide a new highly disordered phase [26,27]. The overall lithium insertion in nickel oxide proceeds up to a very large amount, namely to about 100 mC cm^{-2}.

A similar order-disorder transition, associated to a dip in the voltage-charge of Fig. 1(f), probably occurs during lithium insertion in the indium tin oxide sample. This dip is seen, however, at a charge of only 1.5 mC cm^{-2}. Considering that this film is about three times thicker than the nickel oxide film, its lithium charge capacity is at least one order of magnitude smaller than that of NiO_x. The general trend of the

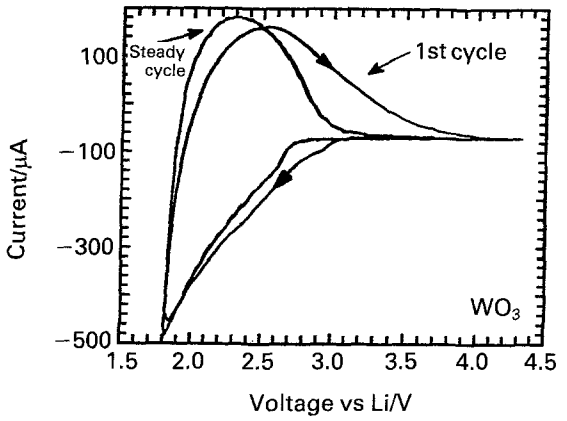

Fig. 2. First voltammogram, and cyclic voltammogram after stabilization for a WO_3 film electrode (0.3 μm thick, area 1 cm^2).

curve in Fig. 1(f) is very complicated and its interpretation is not easy. However, it is relevant to point out that the insertion of lithium in indium tin oxide bulk or thin electrodes has been studied in various laboratories [11,28,29] with contrasting results. This suggests that the characteristics of the process are not typical of the compound but rather depend on sample composition and morphology.

The lithium insertion voltage-charge curves discussed so far were all obtained galvanostatically. The potentiostatic mode was also used in those cases when it was considered of fundamental importance to establish a fixed voltage difference with respect to the lithium reference (for example to prevent deposition of metallic lithium on the electrode and/or to prevent the formation of unwanted phases). These considerations typically apply to the case of nickel oxide, where indeed potentiostatic insertion was often preferred [26].

3.2. *Cyclic voltammetry*

The characteristics of the lithium insertion process in the thin-film oxide electrodes can be conveniently monitored by cyclic voltammetry. As typical examples, Figures 2 and 3 illustrate the repetitive cyclic voltammetry of the WO_3 and ITO electrode, respectively.

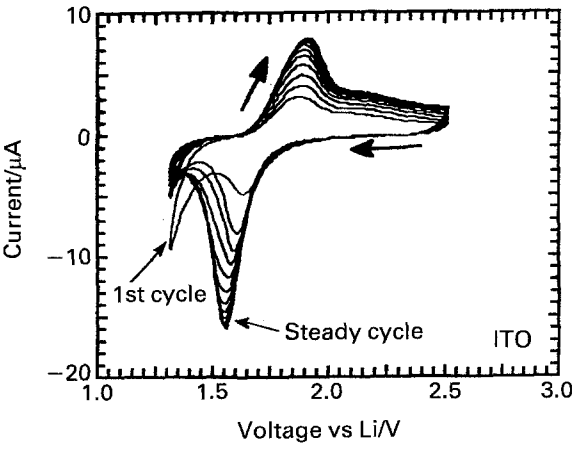

Fig. 3. First voltammogram and subsequent cycles for an ITO thin film electrode (dimensions as in Fig. 2).

In both cases the initial cycles differ, although to a different extent. This suggests that the film electrodes require an activation process to allow a continuous and reversible lithium insertion, and that the type of such activation varies from case to case. For instance, for the oxides investigated here, the activation is a small effect in tungsten oxide (Fig. 2) while it is substantial in indium tin oxide (Fig. 3) and it is crucial in nickel oxide [8]. In the case of the thin film oxides with a polycrystalline structure like V_2O_5, where different phases are formed during lithium insertion, the cyclic voltammetry shows two cathodic and two anodic peaks [30]. Because the cathodic peaks are at the same potentials as the first two plateaux in Fig. 1(a), they appear in the voltammetry of such film when the mixed-phase structures coexist.

It may be assumed that the activation process favours the widening of the structural slabs within which the lithium ions can diffuse. Thus materials with an open crystal structure and well defined channels, such as WO_3 and V_2O_5, are those which require little activation. In fact from the cyclic voltammetry of WO_3 (Fig. 2) the difference between the first cycle and the following stabilized cycle lies essentially in the current tail after the anodic peak, which indicates a faster lithium diffusion in the activated samples than in the as-grown one. At the same time, the charge associated with the peak in the first and in the following cycles remains almost the same. Substantially different is the case of the ITO electrode where the initial voltammetric cycles change dramatically, suggesting that the charge increases consistently as the cycling proceeds to reach steady-state behaviour (Fig. 3). The voltammetric behaviour of nickel oxide [8] is more similar to that of ITO than that of WO_3, indicating the need of substantial activation. Indeed the higher peak current in NiO_x demonstrates a higher charge capacity than ITO.

3.3. *Diffusion kinetics*

The determination of the diffusion of the lithium ions within the solid framework of the oxide host structure is a crucial test for evaluating the applicability of a given insertion electrode. However, measurements of the chemical diffusion coefficient in insertion electrodes are generally difficult to achieve since they are based on the same experimental techniques, and the same interpreting equations which have traditionally been developed for diffusion processes in liquid ionic media. This may lead to inaccurate results. Therefore the diffusion data obtained for the insertion processes in solid oxides have to be interpreted with some care, especially when the electrode consists of a thin film. With this in mind various experimental methods can be considered for the evaluation of the lithium diffusion coefficient in the host oxide electrodes. A common method consists in applying a short galvanostatic pulse to promote excess concentration of the diffusing Li^+ species at the insertion electrode surface and then monitoring the overvoltage-time transient

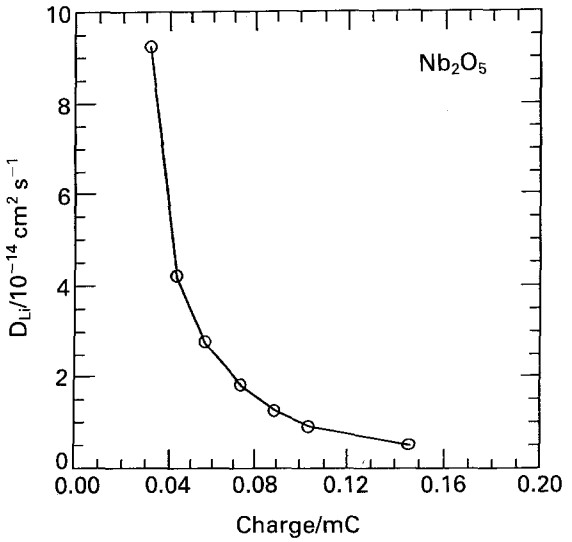

Fig. 4. Li^+ diffusion coefficient versus inserted charge, from the current-step technique.

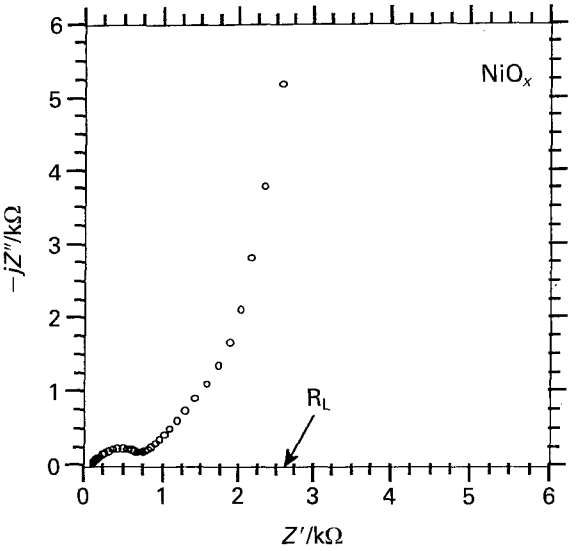

Fig. 5. Impedance plot for a NiO_x film electrode, with 24.4 mC of inserted Li^+ charge (equilibrium potential 1.81 V vs. Li, film 0.06 μm thick, area 1 cm^2).

following the pulse. The data are analysed using a solution of Fick's second law for an instantaneous planar source of diffusing species in a semi- infinite geometry [31] and the chemical diffusion coefficient, D, can be obtained by the equation:

$$D = \left(\frac{4y^2}{p}\right)\left\{I^2\left(\frac{dE}{dq}\right)\Big/\left(\frac{dV}{d(t^{1/2})}\right)\right\} \qquad (13)$$

where y is the thickness of the electrode, I the pulse current, dE/dq the open circuit voltage-charge variation, $dV/d(t^{1/2})$ the voltage-square root of pulse time variation, and t the pulse time. Other symbols have their usual meaning.

Using this technique we have evaluated the diffusion coefficient of lithium in Nb_2O_5 thin film electrodes at different charges. Figure 4 shows the results: the Li^+ diffusion coefficient decreases as the cation concentration increases and this behaviour, combined with the average low value of D (i.e. of the order of $10^{-14}\,cm^2\,s^{-1}$), suggests that the kinetics of the lithium insertion process in Nb_2O_5 is diffusion-controlled and thus that the applications of this electrode are likely to be limited to low-rate regimes and slow devices.

Another popular method to evaluate diffusion in the solid state is impedance spectroscopy, a technique which appears to be very convenient for ion transport studies in those cases, often in thin-film electrodes, where semi-infinite diffusion boundary conditions do not hold. Basically the method consists of the analysis of the impedance response of a given electrode to a small, variable-frequency, a.c. potential perturbation. In the low-frequency range, the response becomes representative of mass transport and, using appropriate circuit analysis [7], the diffusion coefficient, D, can be evaluated. For instance at very low frequencies, namely under the conditions where $f \ll y^2/D$, the impedance response plotted in terms of the imaginary ($-jZ''$) part against the real (Z') part of the total impedance, approaches a $\pi/4$ straight line. Under such a limiting regime, the diffusion coefficient may be evaluated by the following equation:

$$D = \frac{y^2}{3R_L C_L} \qquad (4)$$

where y is the thickness of the electrode film and R_L and C_L are the limiting low frequency resistance and capacitance.

As an example, Fig. 5 illustrates the impedance response of a nickel oxide thin film electrode: R_L and C_L can be obtained by extrapolating the low frequency, $\pi/2$ line to the real axis, thus allowing evaluation of the lithium diffusion coefficient as $D = 4 \times 10^{-12}\,cm^2\,s^{-1}$.

This value is two orders of magnitude higher than that for the Nb_2O_5 electrode but still lower than that for WO_3, often quoted of the order of $10^{-10}\,cm^2\,s^{-1}$ [7]. Therefore, one can conclude from the diffusion data that ion transport in a solid framework is generally a slow process and that compounds with wide interconnected channels such as WO_3 are capable of the most promising behaviour, not only in terms of reversibility, but also in terms of Li insertion-deinsertion rate. The adoption of the thin-film configuration for the electrode means that the diffusion process from the electrochemical interface to the back contact, typically 10^{-5} cm away, takes only one minute or less, even with the low diffusion coefficients as above. The time required to reach an equilibrium condition is therefore considerably shorter than with pellet electrodes, and even galvanostatic discharge curves like those shown in Figs. 1(a)–(f) can be considered, in most cases, to be the result of quasi-equilibrium experiments.

3.4. *Mechanical stress*

It is well known [32] that electrochemical insertion processes modify the bulk properties of the host

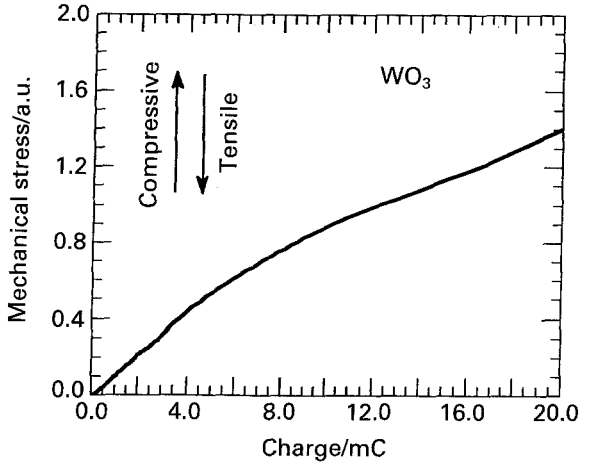

Fig. 6. Mechanical stress variation against charge of the WO_3 film electrode during lithium insertion, as described in Fig. 3.

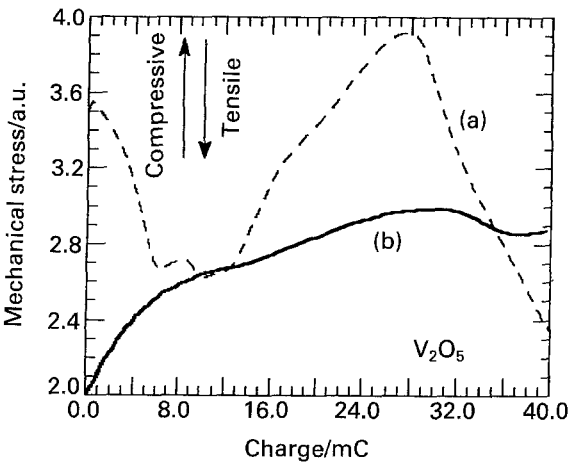

Fig. 7. (a) Mechanical stress versus charge of the V_2O_5 film electrode during Li^+ insertion, as described in Fig. 1. Dashed line: 1st cycle. Solid line: 2nd cycle. (b) Same as above, but for an amorphous film electrode.

materials. Accordingly, upon insertion of lithium the oxide film electrodes tend to change their volume to accommodate the guest ions. However, because of the rigid bonding to the substrate, the only direction in which the film is free to expand or contract is perpendicularly to the substrate plane. As a consequence of this, internal stress is induced in the film and the measurements of this phenomenon provides important information for the clarification of the insertion mechanism [15,27]. For instance, in the simple model of a uniform, isotropic film, it is evident that lithium insertion should promote a volume expansion of the film and, therefore, an internal compressive stress. Such a compressive stress should be a linear function of the charge inserted, provided that no phase transition occurs. This behaviour has indeed been observed for Li_xWO_3 samples (Fig. 6), in accordance with the voltage-charge curve (Fig. 1(d)) which effectively suggested a single-phase, Li-insertion process. The same has been observed for Li insertion in NiO_x and ITO thin films [26]. This is also analogous to what was observed when a palladium film was charged with a few atomic percent of hydrogen [14], using the same technique for the measurement of the stress changes as in the present work.

The situation for multiphase processes in polycrystalline films such as that of V_2O_5 crystalline samples is different. Figure 7 (dashed curve) shows that the initial stress variation upon Li insertion is not compressive but tensile. The explanation is complicated by the fact (i) that the film was grown with a preferential orientation (c-axis perpendicular to the substrate), and (ii) that the oxide is not isotropic, presenting layers along which the guest ions spread. During lithium insertion the unit cell of the oxide lattice may expand in one direction (along the c-axis) whereas it may stay the same or even contract in others. The net result we observed is the rapid build-up (within the first $10\,mC\,cm^{-2}$) of a tensile stress of the film in the plane of the substrate, which induces the bending of the whole sample. The larger the lithium charge, the more complicated and irreversible are the structural changes in the oxide internal structure. The minima at 6 mC and at 12 mC and the maximum at 28 mC in the curve of Fig. 7 can be associated with phase transitions which are known to occur in bulk $Li_xV_2O_5$ crystalline samples at $x = 0.4$, $x = 0.9$ and $x = 2$ [33,34]. A detailed discussion of the mechanical stress changes in vanadium oxide films and of the structural changes during Li^+ insertion, as deduced by X-ray diffraction, will be reported elsewhere [18]. Curve b in Fig. 7 refers to the stress variation during the second insertion cycle in V_2O_5, which is typical of amorphous samples where the process of inserting an ion corresponds to a compressive stress increase of the whole sample structure. This difference between first and second cycle again confirms the conclusions drawn from the corresponding voltage-charge curves (compare Fig. 1(a) and (b)). That is, the deep lithium discharge process occurring in the first cycle changes the oxide material structure from crystalline (ordered with respect to the plane of the supporting glass substrate) into a disordered, amorphous morphology where the lithium insertion occurs without detectable phase transitions.

3.5. *Optical absorption*

The as-grown, lithium-free, thin-film oxide electrodes studied here, with the sole exception of nonstoichiometric nickel oxide in which both the transparent NiO and the absorbing Ni_3O_4 phases coexist [35], are all transparent or semi-transparent to the visible light (514.5 nm).

Lithium insertion is accompanied by electron injection (see the process described in [1]) and, as a consequence, the electronic distribution and the optical absorption of the Li-inserted oxide films change. The changes in colour of the host oxides can thus be conveniently exploited for the realization of electrochromic windows and mirrors designed for a variety of applications in the field of light transmission and control. Again important differences exist between the optical absorption properties of

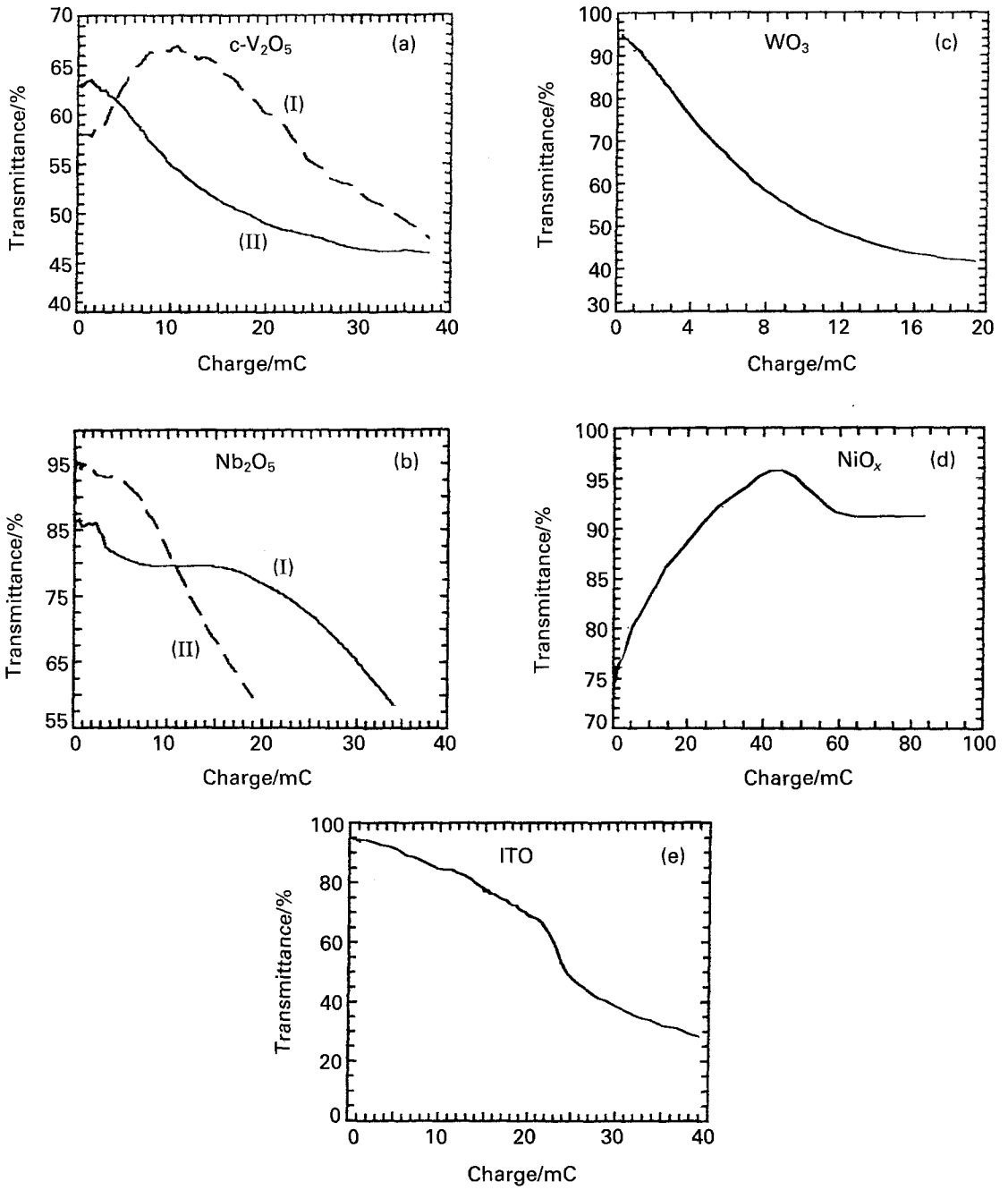

Fig. 8. (a) Optical transmittance versus charge curve during galvanostatic Li^+ insertion for the crystalline V_2O_5 film electrode described in Fig. 1(a). (b) Same as above during galvanostatic Li^+ insertion for the Nb_2O_5 film electrode described in Fig. 1(c). Solid line: as grown. Dashed line: after heat treatment. (c) Same as above during galvanostatic Li^+ insertion for the WO_3 film electrode as described in Fig. 1(d). (d) Same as above during galvanostatic Li^+ insertion for the NiO_x film electrode described in Fig. 1(e). (e) Same as above during galvanostatic Li^+ insertion for the ITO film electrode described in Fig. 1(f).

the crystalline and the amorphous samples of the same metal oxide, as can be clearly seen in Fig. 8. This is because lithium insertion increases enormously the density of conduction electrons and the optical response approaches that of free carriers, but only in the case of ideal crystals. In the real oxide samples, the more disordered the structure of the thin film, the more affected are the optical properties by grain boundary scattering and impurity scattering, and the farther is the optical absorption from that of completely free carriers in the semiconducting oxide energy band structure. The exact physical mechanism responsible for the light absorption in lithiated oxides has been debated in many papers and various theories involving free carrier absorption and small polarons [36] have been invoked. The oxides described in the present work are all cathodically colouring electrodes, with the exception of the NiO_x, which is anodically colouring. To establish the effective visible impact of a given oxide film, it is of relevant importance to monitor its changes in optical transmittance upon lithium insertion. Figure 8(a) illustrates the results for crystalline (curve I) and amorphous (curve II) V_2O_5. Figure 8(b) shows the results for amorphous (curve I) and heat-treated (curve II) Nb_2O_5 and Fig. 8(c), (d) and (e) refer to the transmittance of amorphous WO_3, NiO_x and ITO thin film electrodes, respectively. Among these thin films, tungsten

oxide is the one that in the visible light darkens more per unit charge inserted (Fig. 8(c)) and, therefore, this oxide is the ideal candidate as the optically active electrode in electrochromic displays. The other oxides which darken much less, at least during the initial period of the lithium insertion process, can be regarded as optically passive electrodes [37], also of importance for the realization of complete light transmission devices, such as electrochromic windows [38]. Typical examples are nickel oxide (Fig. 8(d)), vanadium oxide (Fig. 8(a)) and indium tin oxide: the latter remains almost transparent upon lithium insertion up to about $15\,mC\,cm^{-2}$, beyond which, an irreversible reaction and rupture of the film occurs (Fig. 8(e)). In addition to tungsten oxide, amorphous niobium oxide colours cathodically, but its transmittance change is much less than that of WO_3. Therefore, all these optically passive or weakly colouring oxides can be considered quasi-transparent electrodes and used as complementary systems to WO_3 for the fabrication of electrochromic windows as shown in the literature [39].

4. Conclusions

According to the type and the morphology of the oxides in this study some appear more suitable than others for use as thin-film electrodes in novel and rechargeable lithium batteries. Typical is V_2O_5 which, in combination with lithium metal, gives cells with o.c.v. values of the order of 3.5 V and a theoretical energy density as high as $1300\,Wh\,kg^{-1}$. This oxide exhibits facile lithium insertion and behaves as a convenient optically passive, almost fully transparent, film electrode. On the other hand, the other oxides studied show very promising performance as electrochromic materials, both as primary electrodes (e.g. WO_3) and as optically passive complementary electrodes (e.g. ITO and NiO_x), although they are not as promising as V_2O_5 as battery electrodes. ITO remains the oxide layer with the highest sheet conductivity, and is therefore an excellent electronic transparent coductor, but shows relatively little lithium charge capacity; NiO_x has a much larger lithium charge capacity but slow diffusion kinetics. Recent results by Campet *et al.* [40] have shown that new compositions such as $Li^{+}_{0.6}Ni^{II}_{0.7}O^{2-}$ can be prepared electrochemically and show improved kinetics and charge capacity with respect to sputtered NiO_x. Several companies now use some variety of nickel oxide as electrode in their commercially available electrochromic devices. Nb_2O_5 is a new Li^+ insertion material, which deserves further investigation in the future. The most relevant characteristics of WO_3 as a superior electrochromic electrode is its high electrochromic efficiency. This parameter, defined as the ratio between optical density and injected charge, can be experimentally derived from the slope of the linear part of the absorbance-charge curve (derived from the transmittance-charge plot in Fig. 8(d)), and is equal to $15\,cm^2\,C^{-1}$. This value justifies the role of thin-film tungsten oxide as the most popular and almost indispensable primary electrochromic electrode in many optical devices.

Acknowledgements

The authors wish to thank Dr Anne Andersson of the Chalmers Technical University in Göteborg, Sweden, and A. Talledo of the UNI in Lima, Peru, for having kindly provided some of the oxide samples. Ms Rosanna Pileggi is acknowledged for the impedance measurements. Furthermore, F. Decker acknowledges the financial support from the Ministry of Education, MURST 60%.

References

[1] K. M. Abraham, *J. Power Source* **7** (1981) 1.
[2] R. J. Cava, D. W. Murphy and S. M. Zahurak, *J. Electrochem. Soc.* **130** (1983) 2345.
[3] J. P. Pereira-Ramos, R. Messina, C. Piolet and J. Devynck, *Electrochim. Acta* **33** (1988) 1003.
[4] M. S. Whittingham, *Progr. Solid State Chem.* **12** (1978) 1.
[5] J. Desilvestro and O. Haas, *J. Electrochem. Soc.* **137** (1990) 5C.
[6] B. Scrosati, *in* 'Electrochemistry of Novel Materials' (edited by J. Lipkowski and P. Ross), VCH, New York, in press.
[7] C. Ho, I. D. Raistrick and R. A. Huggins, *J. Electrochem. Soc.* **127** (1980) 343.
[8] S. Passerini, B. Scrosati and A. Gorenstein, *ibid.* **137** (1990) 3297.
[9] A. Talledo, A. M. Andersson and C. G. Granqvist, *J. Appl. Phys.* **69** (1991) 3261.
[10] S. F. Cogan, E. J. Anderson, T. D. Plante and R. D. Rauh, *Appl. Opt.* **24** (1985) 2282.
[11] A. Corradini, A. M. Marinangeli and M. Mastragostino, *Electrochim. Acta* **35** (1990) 1757.
[12] W. Estrada, A. M. Andersson and C. G. Granqvist, *J. Appl. Phys.* **64** (1988) 3678.
[13] B. A. Boukamp, *Solid St. Ionics* **20** (1986) 31.
[14] S. N. Sahu, J. Scarminio and F. Decker, *J. Electrochem. Soc.* **137** (1990) 1150.
[15] J. Scarminio, W. Estrada, A. Andersson, A. Gorenstein, F. Decker, *ibid.* **139** (1992) 1236.
[16] C. Cartier, A. Tranchant, M. Verdaguer, R. Messina and H. Dexpert, *Electrochim. Acta* **35** (1990) 889.
[17] M. Nabavi, C. Sanchez, F. Taulelle, J. Livage and A. de Guibert, *Solid State Ionics* **28–30** (1988) 1193.
[18] J. Scarminio, S. Passerini, F. Decker, A. Talledo and A. A. Andersson, *Electrochim. Acta* **38** (1993) 1637.
[19] Y. Sakurai and J. Yamaki, *J. Electrochem. Soc.* **132** (1985) 512.
[20] M. Green, *Thin Sol. Films* **50** (1978) 145.
[21] N. Yoshiike, Y. Mizuno and S. Kondo, *J. Electrochem. Soc.* **131** (1984) 2634.
[22] W. C. Dautremont-Smith, M. Green and K. S. Kang, *Electrochim. Acta* **22** (1977) 751.
[23] H. R. Zeller and H. U. Beyeler, *Appl. Phys.* **13** (1977) 231.
[24] P. Kulesza and L. R. Faulkner, *J. Electroanal. Chem.* **248** (1977) 305.
[25] M. Green and K. S. Kang, *Solid State Ionics* **8** (1983) 281.
[26] F. Decker, S. Passerini, R. Pileggi and B. Scrosati, *Electrochim. Acta* **37** (1992) 1033.
[27] F. Decker, R. Pileggi, S. Passerini and B. Scrosati, *J. Electrochem. Soc.* **138** (1991) 3182.
[28] R. B. Goldner, G. Foley, E. L. Goldner, P. Norton, K. Wong, T. Haas, G. Seward and R. Chapman, *Appl. Opt.* **24** (1985) 2283.
[29] J. S. E. M. Svensson and C. G. Granqvist, *Appl. Opt.* **24** (1985) 2284.
[30] S. F. Cogan, *in* 'Large Area Chromogenics: Materials and Devices for Transmittance Control', (edited by C. M. Lampert and C. G. Granqvist), SPIE Optical Engineering Press, Bellingham, MA (1990) p. 313.

[31] W. Weppner and R. A. Huggins, *J. Electrochem. Soc.* **124** (1977) 1569.
[32] A. M. Chippindale, P. G. Dickens and A. V. Powell, *Prog. Solid St. Chem.* **21** (1991) 133.
[33] R. J. Cava, A. Santoro, D. W. Murphy, S. M. Zahurak, R. M. Fleming, P. Marsch and R. S. Roth, *J. Solid State Chem.* **65** (1986) 63.
[34] J. M. Cocciantelli, M. Ménétrier, C. Delmas, J. P. Doumerc, M. Pouchard and P. Hagenmuller, *Solid State Ionics* **50** (1992) 99.
[35] A. Andersson, W. Estrada, C. G. Granqvist, A. Gorenstein and F. Decker, *in* Proc. Int. Symp. SPIE, the Hague, Netherlands (1990) Vol. 1272, p. 96.
[36] F. P. Koffyberg and F. A. Benko, *Phil. Mag.* **B38** (1978) 357.
[37] A. Talledo, A. M. Andersson and C. G. Granqvist, *J. Mater. Res.* **5** (1990) 1253.
[38] M. Mizuhashi, J. Nagai, and T. Kamimori, *in* 'Large Area Chromogenics: Materials and Devices for Transmittance Control' (edited by C. M. Lampert and C. G. Granqvist), SPIE Optical Engineering Press, Bellingham, MA (1990) p. 494.
[39] S. Passerini, B. Scrosati, A. M. Andersson and C. G. Granqvist, *J. Electrochem. Soc.* **136** (1989) 3394.
[40] G. Campet, B. Morel, M. Bourrel, J. M. Chabango, D. Ferry, R. Garie, C. Quet, C. Geoffrey, J. J. Videau, J. Portier, C. Delmas and J. Salardenne, *Mat. Sci. Engineer.* **B8** (1991) 303.